

# Statistical Properties of the one dimensional Anderson model relevant for the Nonlinear Schrödinger Equation in a random potential

Erez Michaely and Shmuel Fishman

August 19, 2021

Physics Department, Technion - Israel Institute of Technology, Haifa 32000, Israel

## Abstract

The statistical properties of overlap sums of groups of four eigenfunctions of the Anderson model for localization as well as combinations of four eigenenergies are computed. Some of the distributions are found to be scaling functions, as expected from the scaling theory for localization. These enable to compute the distributions in regimes that are otherwise beyond the computational resources. These distributions are of great importance for the exploration of the Nonlinear Schrödinger Equation (NLSE) in a random potential since in some explorations the terms we study are considered as noise and the present work describes its statistical properties.

## 1 Introduction

In the present work the statistics of the overlap sums and combinations of the eigenenergies of the one dimensional Anderson model [1, 2] are calculated. These quantities naturally arise in the exploration of the Nonlinear Schrödinger Equation in a random potential [3, 4, 5, 6, 7, 8]. The overlap sums defined by (6) measure the overlap of four eigenfunctions of the Anderson model. The combinations of the eigenenergies dominate the phase of the nonlinear terms. As a result of the nonlinearity such terms that affect the dynamics, play a crucial role in the dynamics of the nonlinear model. Sometimes these terms are considered as effective noise [9, 7, 8]. Their statistical properties are crucial for the effective noise theories. The statistics presented here may be also of interest for mathematicians exploring the Anderson model and related random models. The Nonlinear Schrödinger Equation (NLSE) in a random potential takes the form [3, 4, 5, 7, 8, 6]

$$i\partial_t\psi = H_0\psi + \beta|\psi|^2\psi, \quad (1)$$

where  $H_0$  is the linear part with a disordered potential, which on a lattice takes the form of

$$H_0\psi(x) = -(\psi(x+1) + \psi(x-1)) + \varepsilon(x)\psi(x). \quad (2)$$

In this work it is assumed that  $\varepsilon(x)$  are identical independent random variables (i.i.d) uniformly distributed in the interval of  $[-\frac{W}{2}, \frac{W}{2}]$ . This is the famous Anderson model [1, 2]. Here we study the model in one dimension where all the states are exponentially localized [10, 11]

The NLSE was derived for a variety of physical systems under some approximations. It was derived in classical optics where  $\psi$  is the electric field by expanding the index of refraction in powers of the electric field keeping only the leading nonlinear term [12, 13, 14]. For Bose-Einstein Condensates (BEC), the NLSE is a mean field approximation where the term proportional to the density  $\beta|\psi|^2$  approximates the interaction between the atoms. In this field the NLSE is known as the Gross-Pitaevskii Equation (GPE) [15, 16, 17, 18, 19].

A natural question in this research is whether a wave packet that is initially localized in space will indefinitely spread for dynamics controlled by (1) [3, 4, 5, 7, 8, 6].

It is convenient to expand the wavefunction  $\psi$  in the linear problem eigenfunctions  $u_n$

$$\psi(x, t) = \sum_n c_n(t)u_n(x)e^{-iE_n t} \quad (3)$$

where  $E_n$  is the eigenenergy of the n-th eigenstate. The width of the energy spectrum is  $\Delta = 4 + W$  with  $E_n \in [-2 - \frac{W}{2}, 2 + \frac{W}{2}]$  and  $u_n$  typically falling off exponentially [10, 11]

$$u_n(x) \approx \frac{e^{-|x_n-x|/\xi_n}}{\sqrt{\xi_n}}\varphi(x) \quad (4)$$

where  $\varphi(x)$  is a real random function of order unity,  $\xi_n$  is the localization length for the n-th state and  $x_n$  is its localization center. The expansion coefficients  $c_n(t)$  satisfy [3, 4]

$$i\partial_t c_{m_1}(t) = \beta \sum_{m_2, m_3, m_4} V_{m_1}^{m_2, m_3, m_4} \exp(i \cdot t\Phi_{m_1}^{m_2, m_3, m_4}) c_{m_2}^* c_{m_3} c_{m_4} \quad (5)$$

where

$$V_{m_1}^{m_2, m_3, m_4} = \sum_x u_{m_1}(x)u_{m_2}(x)u_{m_3}(x)u_{m_4}(x). \quad (6)$$

is the overlap sum and

$$\Phi_{m_1}^{m_2, m_3, m_4} = E_{m_1} + E_{m_2} - E_{m_3} - E_{m_4} \quad (7)$$

is the total phase.

The main purpose of this paper is to explore numerically the statistical properties of the overlap sum  $V_{m_1}^{m_2, m_3, m_4}$  and the total phase  $\Phi_{m_1}^{m_2, m_3, m_4}$  as well as of related quantities. We believe that understanding the qualitative properties of  $V_{m_1}^{m_2, m_3, m_4}$  and  $\Phi_{m_1}^{m_2, m_3, m_4}$  will help to build a toy model that may shed light on the spreading mechanism. Of particular interest will be to find universal distributions in terms of scaling variables as explained in Sec. 2. These should be relevant for the entire energy regime. The distributions are found numerically and are a generalization of the distribution of  $V_0^{0,0,0}$  that was found analytically by Fyodorov and Mirlin in a narrow energy range [20]. In Sec. 2 we explore statistical properties of  $V_{m_1}^{m_2, m_3, m_4}$  for weak disorder and in Sec. 3 we will explore statistical properties of  $\Phi_{m_1}^{m_2, m_3, m_4}$  for weak disorder. For weak disorder it is expected from the scaling theory that all statistical properties are determined by the localization length, while for the strong disorder this does not hold [21]. Some results for strong disorder are presented in Sec. 4. The results are summarized and discussed in Sec. 5.

## 2 Statistical properties of $V_{m_1}^{m_2, m_3, m_4}$ for weak disorder

We explore the values of  $V_{m_1}^{m_2, m_3, m_4}$  in the regime of weak disorder (which corresponds to relatively long localization length  $\xi$ ). Most of the explorations are numerical. The lattice size is fixed at  $N = 500$ . For each realization of the  $\varepsilon(x)$ , we computed the eigenfunctions  $u_n$  and ordered them in space by the center of norm coordinate, defined by  $x_n = \sum_x x \cdot u_n^2(x)$ . We choose  $u_{m_1}$  with  $m_1 = 0$  to be the eigenfunction centered in the lattice. We studied only the following quantities  $V_0^{0,0,0}$ ,  $V_0^{0,1,1}$ ,  $V_0^{0,0,1}$ ,  $V_0^{0,1,2}$  and  $V_0^{1,2,3}$  representative of values where  $V_{m_1}^{m_2, m_3, m_4}$  are large. Combinations with  $m_i \gtrsim \xi$  (taking  $m_1 = 0$ ) have negligible values because the overlap sum is a sum of exponentially decaying functions in space of the form of (4). We calculated these values for  $N_R = 2 \cdot 10^4$  realizations, and repeated this calculation for 7 disorder strengths in the weak disorder regime  $1 \leq W \leq 2$  where the maximal localization length  $\xi$  takes the values of  $25 \lesssim \xi \lesssim 103$ . In the regime of weak disorder the maximal localization length is [22]

$$\xi \approx \frac{96}{W^2}. \quad (8)$$

We computed the distributions of the  $V_{m_1}^{m_2, m_3, m_4}$  as follows. We calculated  $2 \cdot 10^4$  values of  $V_{m_1}^{m_2, m_3, m_4}$ , one for each realization. We know that  $|V_{m_1}^{m_2, m_3, m_4}|$  must satisfy  $0 < |V_{m_1}^{m_2, m_3, m_4}| < 1$  because the eigenfunctions are all normalized  $\sum_x u_n^2(x) = 1$ . We made a histogram of the values  $|V_{m_1}^{m_2, m_3, m_4}|$  in number of bins  $N_{bins} = 500$  in the interval  $[0, 1]$ , the resulting bin size is  $\delta x = 0.002$ . In order to get the distribution we normalized the values of the histogram, dividing them by the number of realizations,  $N_R$ .

In the calculation of the statistical properties of the  $V_{m_1}^{m_2, m_3, m_4}$  we distinguish different groups according to the number of different indices  $m_i$ .

### 2.1 The case $m_1 = m_2 = m_3 = m_4 = 0$

In the case where all indices are equal we have chosen them to be zero. In this case

$$V_0^{0,0,0} = \sum_x u_0^4(x) \equiv V_0. \quad (9)$$

It is just the inverse participation ratio. Its distribution was calculated analytically by Fyodorov and Mirlin [20] and was found to satisfy scaling, that is if  $P(V_0, \xi)$  is the probability density of  $V_0$  and the localization length is  $\xi$  then, if one defines a scaling variable

$$y_0 = V_0 \xi \quad (10)$$

its probability density is

$$P(y_0) = \frac{1}{\xi} P(V_0, \xi). \quad (11)$$

In [20] this scaling was found to hold in a *narrow range of energy*. In the present work we demonstrate numerically that it is an excellent approximation also when the maximal localization length (8) is used. The scaling function is different from the one of [20].

First we verify that the average of  $V_0$  satisfies

$$\langle V_0 \rangle = \frac{C}{\xi} \quad (12)$$

where C is a constant independant of  $\xi$ , and  $\xi$  is given by (8), as maybe expected from the scaling relation (in

agreement with [9]). This is clear from Fig. 1, and it is found that  $C = 1.296 \dots$

The probability density function (PDF) as a function of  $V_0$  is presented in Fig. 2a . A typical function fitted to the numerical data is shown in Fig. 2b for  $W = 1$  and it takes the form

$$P(V_0) = c_1 e^{-(c_2 + c_3 \cdot \ln(V_0))^2} \quad (13)$$

with  $c_1 = 127.7 \dots$ ,  $c_2 = 9.097 \dots$  and  $c_3 = 1.865 \dots$ . We found that the scaling (10) and (11) holds for all weak disorder strengths studied as shown in Fig.2c. The resulting scaling function is

$$P(y_0) = a_1 e^{-(a_2 + a_3 \ln(y_0))^2}. \quad (14)$$

with  $a_1 = 1.21 \dots$ ,  $a_2 = 0.539 \dots$  and  $a_3 = 1.71 \dots$

What is the reason for the scaling? From (6) and (4) it is clear that the magnitude of each of the  $u_{m_i}$  is of order  $\frac{1}{\sqrt{\xi_0}}$  while the number of terms in the sum that contribute substantially is of order  $\xi_0$ . Therefore  $V_0$ , although random, it is typically proportional to  $\frac{1}{\xi_0}$ . Note that all the contribution to the sum (6) are positive.

If the calculation is confined to a narrow energy,  $\xi_0$  is practically constant and  $P(y_0)$  is the function found in [20]. In the case we study the energy of the site  $m_1 = 0$  (middle of the lattice) varies as the realizations change and an effective average over the realizations is preformed. Since the density of states (see Fig. 6) and the localization length as a function of energy are flat at the center of the band, where the localization length is maximal and takes the value close to (8), terms with this value of the localization length dominate the overlap sum (6). It is worthwhile to note that the scaling function (14) we found is different from the one found in [20]. It is practically the average of the function found in [20] over energy.

Now we consider the cases where the  $m_i$  take two different values say  $V_0^{0,1,1}$  of  $V_0^{0,0,1}$ .

## 2.2 Distribution of $V_0^{0,1,1}$

Also here an argument similar to the one presented in the previous section holds, but the localization lengths of the two wave functions involved are different, the overlap sum is of the order  $\frac{1}{\xi_0 + \xi_1}$ , therefore  $V_0^{0,1,1}$  behaves as  $\frac{1}{\xi}$ . In order to investigate the distribution of  $V_0^{0,1,1}$ , denoted here by  $V_1$ , which consists of many near zero values, we generated the histogram of  $\ln(V_1)$  rather than  $V_1$ . In Fig. 3 we present the distribution of  $P(\ln(V_1))$  as a function of  $\ln(V_1)$ . The best fit for the scaling function, in terms of the scaling variable

$$y_1 = V_1 \xi \quad (15)$$

is shown there as well. As expected  $\langle V_1 \rangle$  satisfies a relation similar to (12) but with  $C = 0.429 \dots$  (in agreement with [9]).

## 2.3 Distribution of $V_0^{0,0,1}$

Let us denote  $V_0^{0,0,1} \equiv V_2$ . From the definition (6) it is clear that  $\langle V_2 \rangle = 0$ . Therefore to estimate the typical value of  $V_2$  we study  $\langle V_2^2 \rangle$ . It can be estimated by

$$\langle V_2^2 \rangle = \left\langle \left( \sum_x u_0^3(x) u_1(x) \right)^2 \right\rangle \approx \left\langle \left( \sum_x u_0^6(x) u_1^2(x) \right) \right\rangle. \quad (16)$$

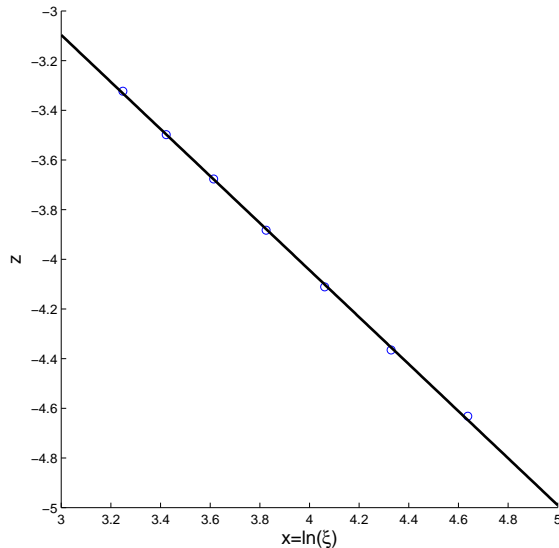


Figure 1: a log-log scale of  $z = \ln(\langle V_0 \rangle)$  as a function of  $x = \ln(\xi)$ . The numerical results are represented by circles while the line is the best fit. The fit is  $z = -a_0x + b_0$  for  $a_0 = 0.95\dots$  and  $b_0 = 0.26\dots$

It is of order  $\frac{1}{\xi_0^2(3\xi_1 + \xi_0)}$ . Therefore it is reasonable that  $\langle V_2^2 \rangle \sim \frac{1}{\xi^3}$ . Indeed one finds

$$\sqrt{\langle V_2^2 \rangle} = \bar{C}\xi^{-1.5} \quad (17)$$

with  $\bar{C} = 0.566\dots$  independent of  $\xi$ . This motivates us to introduce the scaling variable

$$y_2 = V_2\xi^{1.5}. \quad (18)$$

In Fig. 4 we show the distribution of  $P(\ln(V_2^2))$  as a function of  $\ln(V_2^2)$  in terms of the scaling variable  $y_2$ .

## 2.4 Distribution of $V_{m_1}^{m_2, m_3, m_4}$ when 3 or 4 different $m_i$ are involved

In this case we could not find any simple scaling relation. The averages are found to be exponential in  $\xi$ , as one can see from Fig. 5

## 3 Statistical properties of $\Phi_n^{m_1, m_2, m_3}$ for weak disorder

In this section we explore the statistical properties of  $\Phi$  defined in Sec. 1 and the distribution of the eigenenergies  $E_n$ . For the weak disorder regime we fixed the lattice size  $N = 500$  and computed the eigenenergies for  $N_R = 10^3$  realizations. We repeated this calculation for 7 different values of the disorder strength,  $1 < W < 2$  which correspond to  $25 \lesssim \xi \lesssim 103$ .

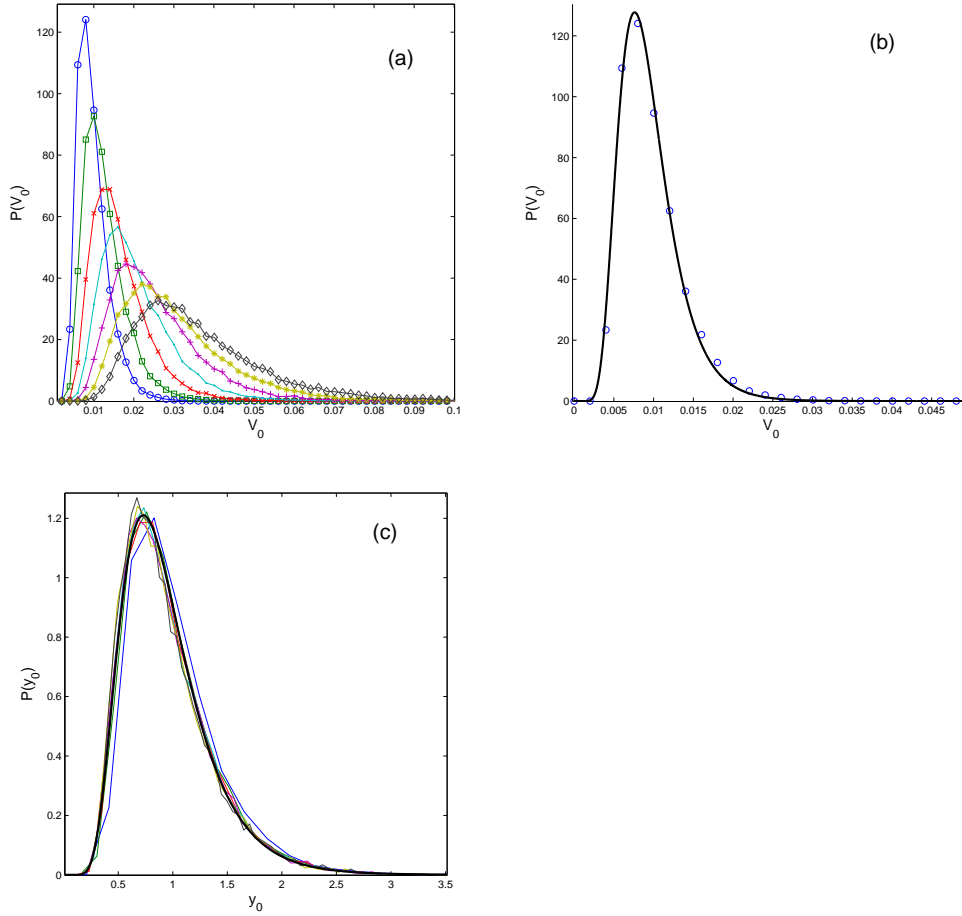


Figure 2: The PDF for various values of weak disorder strength. (a) The PDF as a function of  $V_0$  for: blue circles  $W = 1$  ( $\xi \approx 103$ ), green squares  $W = 1\frac{1}{6}$  ( $\xi \approx 75$ ), red crosses  $W = 1\frac{1}{3}$  ( $\xi \approx 58$ ), turquoise dots  $W = 1\frac{1}{2}$  ( $\xi \approx 46$ ), purple pluses  $W = 1\frac{2}{3}$  ( $\xi \approx 37$ ), green stars  $W = 1\frac{5}{6}$  ( $\xi \approx 30$ ), black rhombus  $W = 2$  ( $\xi \approx 25$ ). (b) The PDF for  $W = 1$ , the results of the simulation are presented by blue circles, while the solid line is given by (13). (c)  $P(y_0)$  as a function of  $y_0$ . The data collapse indicates the scaling of the PDF with the localization length  $\xi$ . The colored lines correspond to various values of the disorder strength. The black thick line is the best fit for the log normal distribution (14).

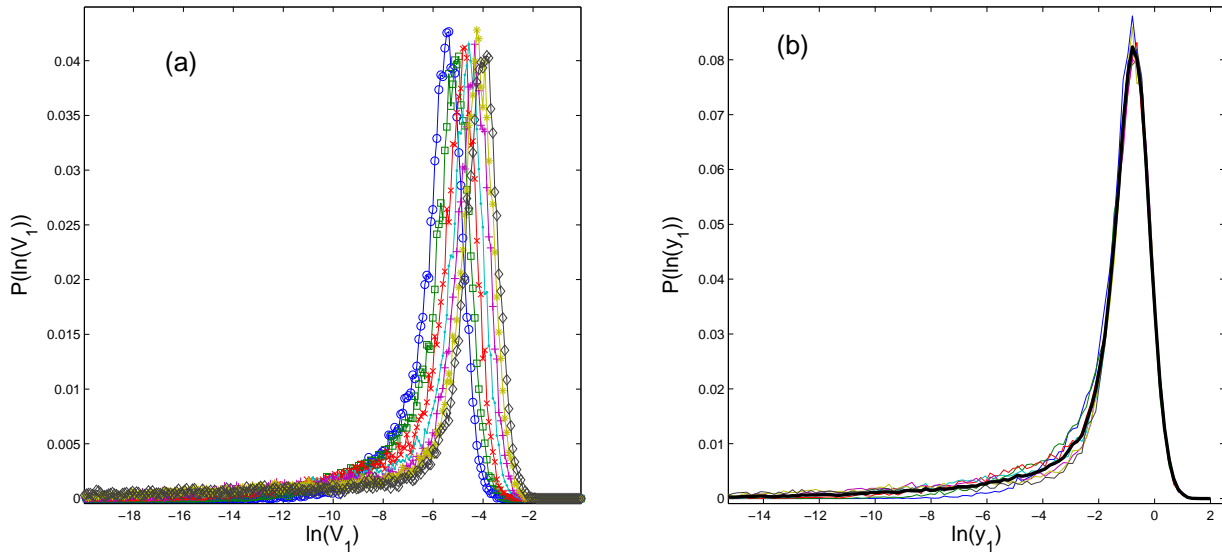


Figure 3: The PDF of  $\ln(V_1)$  for various values of weak disorder strength presented in Fig 2. (a) The PDF as a function of  $\ln(V_1)$  (b) The scaled PDF as a function of  $\ln(y_1)$  the black thick line represents the best fit. The data collapse indicates the scaling of the PDF with the localization length  $\xi$ . The colored lines correspond to various strengths of disorder.

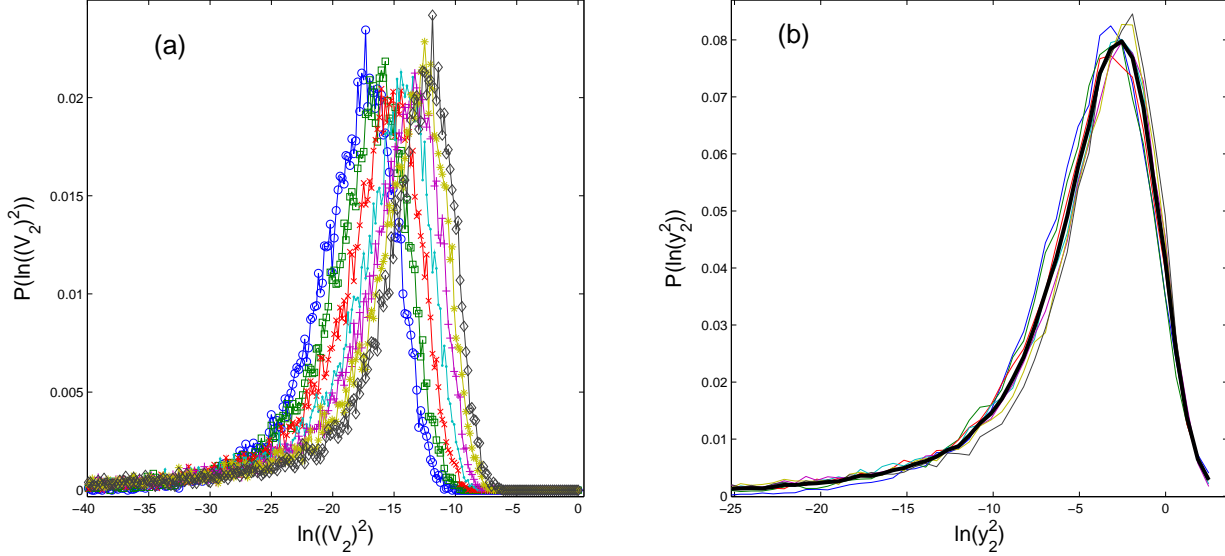


Figure 4: As in Fig. 3 the PDF of  $\ln(V_2^2)$  for various values of weak disorder strength presented there. (a) The PDF as a function of  $\ln(V_2^2)$ . (b) The scaled PDF as a function of  $\ln(y_2^2)$ . The black thick line is the best fit. The number of bins here is 200.

### 3.1 Distribution of $E_n$

The distribution of the eigenenergies for the weak disorder regime, as plotted in Fig. 6 is symmetric around  $E = 0$  and characterized by convex function in the middle and sharply decaying function at the boundaries.

### 3.2 Distribution of $\Phi^+ \equiv E_n + E_m$

We calculated the distribution of the sums of two eigenenergies obtained for the same realization. The motivation for calculation of these sums is from the terms where  $m_1 = m_2 = 0$  and  $m_3, m_4$  are arbitrary in (5). In Fig. 7 we plot distributions of  $\Phi^+$  with various disorder strengths. Note the maximal value of the distribution decreases with  $W$ . We found the following relation between the maximal value of the distribution which we will denote  $\Phi_m$  and  $\xi$ ,

$$\Phi_m(\xi) = 0.13\xi^{0.15} \quad (19)$$

### 3.3 Distribution of $\Phi^- \equiv E_n - E_m$

We calculated the distribution of the differences between two eigenenergies obtained for the same realization. Despite the symmetric nature of the distribution of  $E_i$  the value of  $\Phi^-$  differs from  $\Phi^+$  because of level repulsion [23, 24]. Therefore we anticipate a relatively large peak at  $\Phi^- = 0$ , as shown in Fig. 8. A comparison between  $\Phi^-$  and  $\Phi^+$  is presented in Fig. 9. One can see that, the distributions differ substantially only near  $\Phi^- = 0$  and  $\Phi^+ = 0$



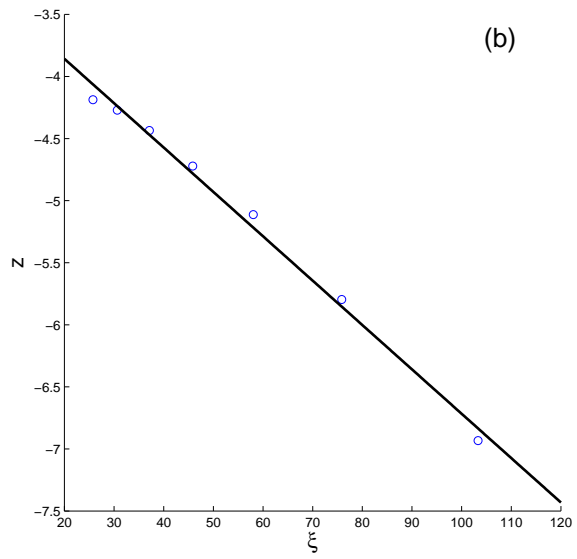
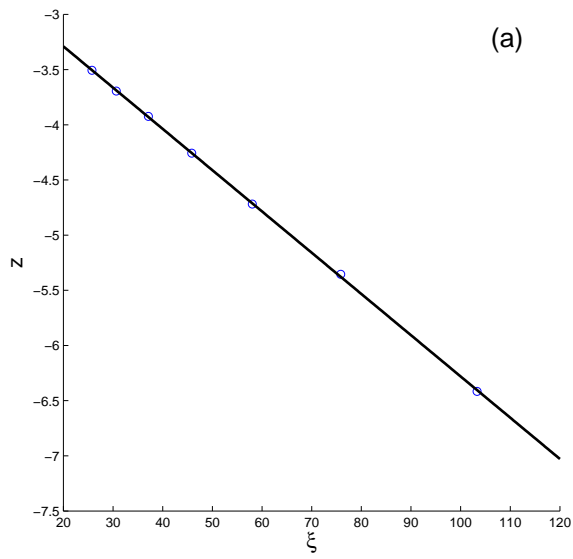


Figure 5: (a)  $z = \ln \sqrt{\langle (V_0^{0,1,2})^2 \rangle}$  as a function of  $\xi$ . The fit is  $z = -0.037 \cdot \xi - 2.5$  (b)  $z = \ln \sqrt{\langle (V_0^{1,2,3})^2 \rangle}$  as a function of  $\xi$ . The fit is  $z = -0.036 \cdot \xi - 3.1$

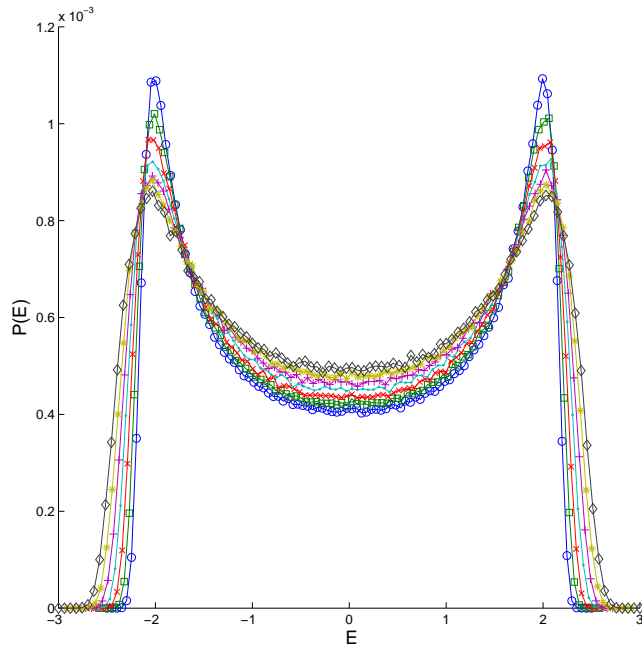


Figure 6: The PDF of  $E_n$  for various weak disorder strength. blue circles  $W = 1$  ( $\xi \approx 103$ ), green squares  $W = 1\frac{1}{6}$  ( $\xi \approx 75$ ), red crosses  $W = 1\frac{1}{3}$  ( $\xi \approx 58$ ), turquoise dots  $W = 1\frac{1}{2}$  ( $\xi \approx 46$ ), purple pluses  $W = 1\frac{2}{3}$  ( $\xi \approx 37$ ), green stars  $W = 1\frac{5}{6}$  ( $\xi \approx 30$ ), black rhombus  $W = 2$  ( $\xi \approx 25$ ).

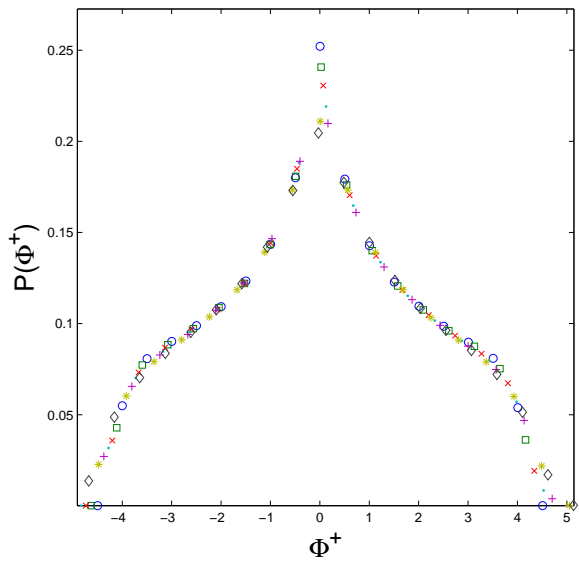


Figure 7: The distribution of  $\Phi^+$  for strengths of disorder as in Fig. 6 using the same symbols.

because of level repulsion.

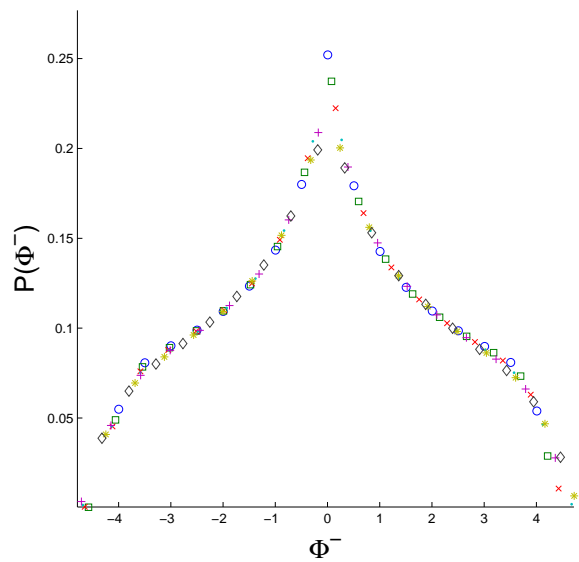


Figure 8: (a) The distribution of  $\Phi^-$  for strengths of disorder as in Fig. 6. Number of bins used is 100.

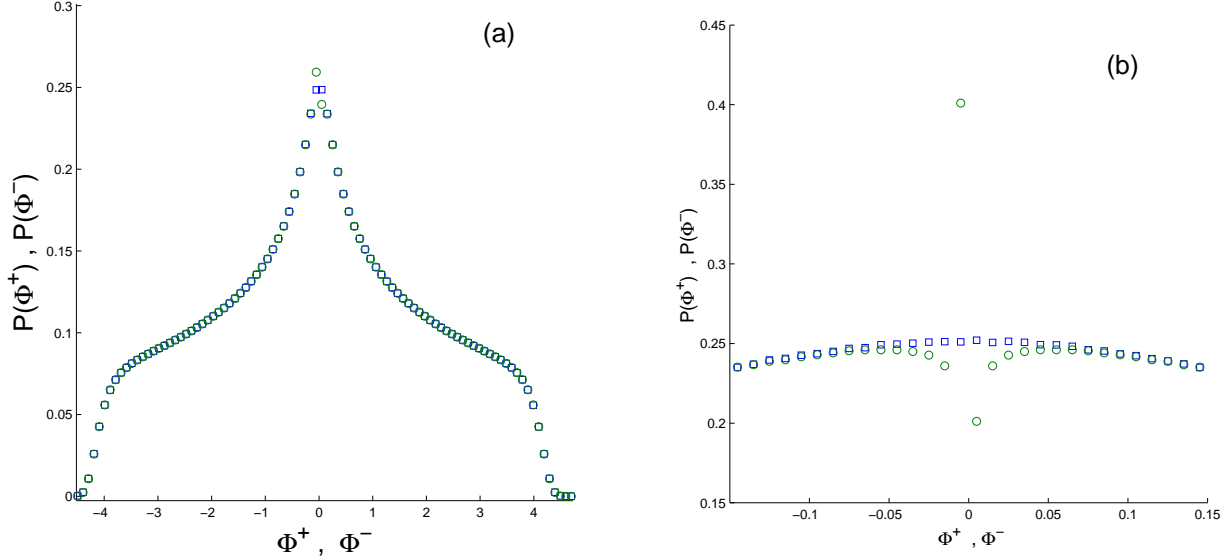


Figure 9: (a) The PDF of  $\Phi^+$  (blue squares) and  $\Phi^-$  (green circles) for  $W = 1$ , total number of bins used is  $10^2$ . (b) zoom of (a) around  $\Phi^+ = 0$  and  $\Phi^- = 0$ , total number of bins used is  $10^3$ .

### 3.4 Distribution of $\Phi_{m_1}^{m_2, m_3, m_4}$

$\Phi_{m_1}^{m_2, m_3, m_4} = \Phi$  is a combination of 4 eigenenergies. In order to calculate the distribution of  $\Phi$  one needs to compute  $N^4$  of these combinations. To avoid lengthy computations we are presenting a much smaller number of realizations and use a smaller lattice size. In this subsection we will present these distribution for  $N_R = 10$  realizations on a lattice with size  $N = 128$  for 7 disorder strengths in the range  $1 \leq W \leq 4$ , which correspond to  $6.5 < \xi < 103$ . A Gaussian like distribution is found for all values of  $W$ , as shown in Fig. 10a. The form of the distribution is

$$P(\Phi) = A e^{-\frac{\Phi^2}{\sigma^2}} \quad (20)$$

where  $A$  is the normalization constant and  $\sigma$  is the width of the gaussian. A fit is presented in Fig. 10b for  $W = 1$  with the values of  $A = 0.1335\dots$  and  $\sigma = 4.278\dots$  in agreement with [4]. Next we calculated the width of each Gaussian  $\sigma$  as a function of  $\xi$  and found

$$\sigma(\xi) = b_1 \cdot \xi^{-b_2} + b_3 \quad (21)$$

with  $b_1 = 5.924\dots$ ,  $b_2 = 0.865\dots$  and  $b_3 = 4.17\dots$ , this function is presented in Fig. 10c. For the case of very weak disorder,  $\xi \gg 1$ , we see the value of  $\sigma$  approaches  $\sigma \rightarrow 4.17\dots$ , which is in agreement with the value found for the distribution plotted in Fig. 10d where  $W = 0$ .

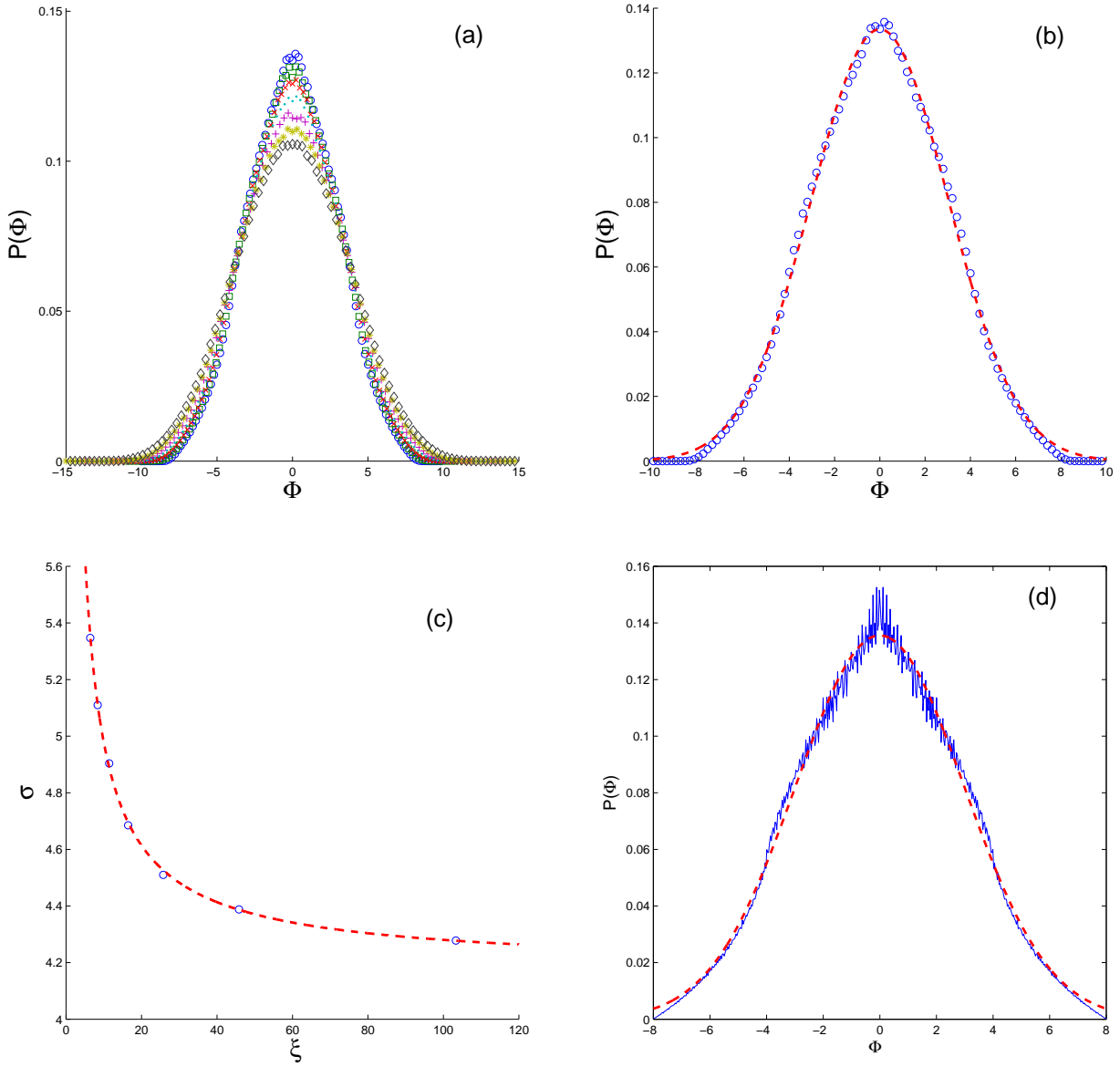


Figure 10: The PDF of  $\Phi$  for various values of weak disorder strength. (a) blue circles  $W = 1$  ( $\xi \approx 103$ ), green squares  $W = 1\frac{1}{2}$  ( $\xi \approx 46$ ), red crosses  $W = 2$  ( $\xi \approx 25$ ), turquoise dots  $W = 2\frac{1}{2}$  ( $\xi \approx 16.5$ ), purple pluses  $W = 3$  ( $\xi \approx 11.4$ ), green stars  $W = 3\frac{1}{2}$  ( $\xi \approx 8.4$ ), black rhombus  $W = 4$  ( $\xi \approx 6.5$ ). Number of bins = 1000. (b) the PDF as a function of  $\Phi$  with  $W = 1$ , the red dashed line is the fit (20). (c)  $\sigma$  as a function of  $\xi$ , the red dashed line it the fit 21. (d) The PDF as a function of  $\Phi$  for  $W = 0$ , the red dashed line it the fit (20) with values  $A = 0.1335$  and  $\sigma = 4.27$ .

## 4 Strong disorder

In the case of strong disorder one does not expect scaling to work [21]. Indeed we could not find a scaling distribution for  $V_0$  and  $V_1$  defined in Sec. 2 for the regime of strong disorder. Their averages scale with different powers of  $\xi$  as is clear from Fig. 11. The distribution of the  $E_n$  exhibits a maximum near  $E = 0$  as one can see from Fig. 12, while for weak disorder a minimum is found there (compare Fig. 6 to Fig. 12). The distributions of  $\Phi^+$  and  $\Phi^-$  presented in Fig 13 exhibit a linear dependence on the values of  $\Phi^+$  and  $\Phi^-$  respectively. The distribution of  $\Phi$  is similar to the one found for weak disorder, Fig. 10b fits even better gaussian distribution.

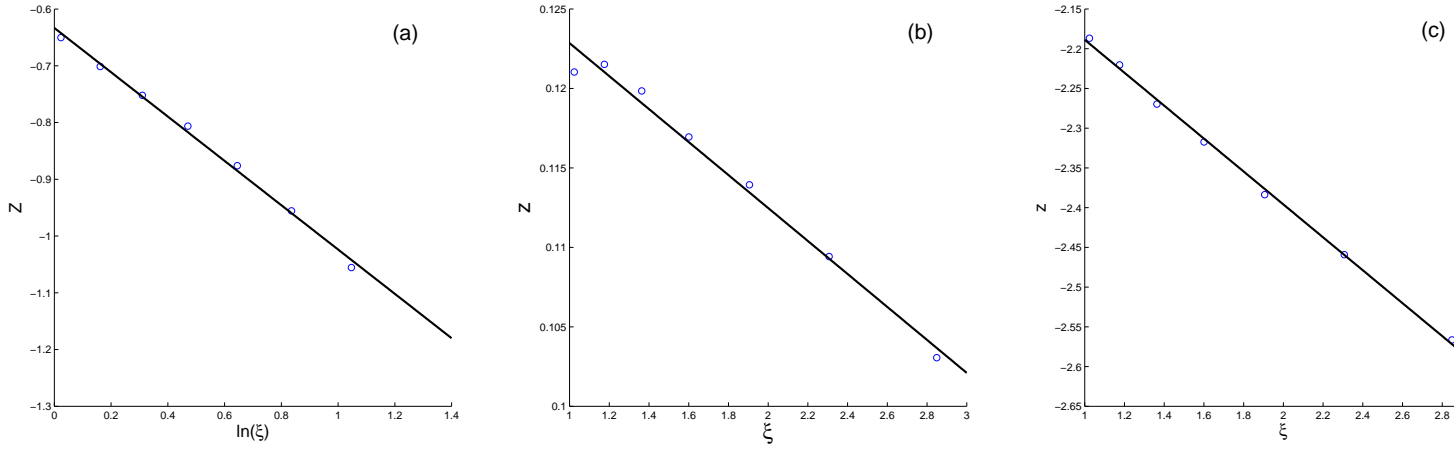


Figure 11: (a)  $z = \ln(\langle V_0 \rangle)$  as a function of  $\ln(\xi)$  with a linear fit  $z = -0.39 \cdot \ln(\xi) - 0.63$ . (b)  $z = \langle V_1 \rangle$  as a function of  $\xi$  with the fit  $z = -0.01 \cdot \xi + 0.13$ . (c)  $z = \ln(\langle V_2 \rangle)$  as a function of  $\xi$  with a linear fit  $z = -0.21 \cdot \xi - 2$

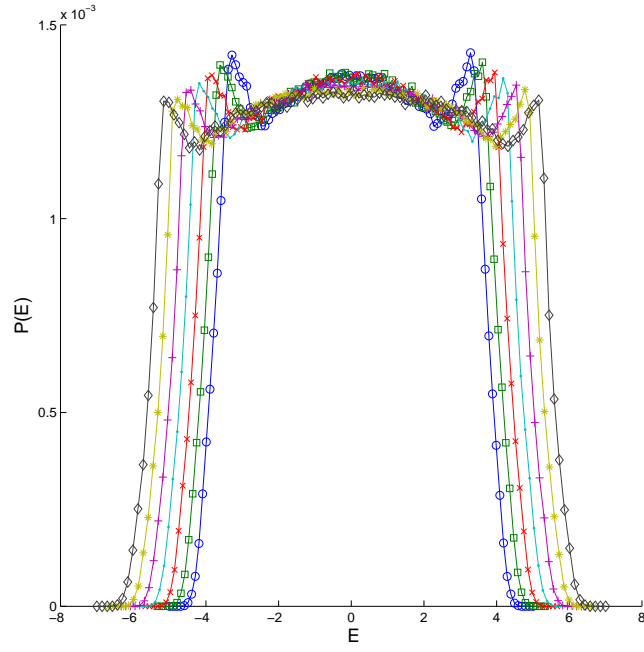


Figure 12: The PDF of  $E_n$  for various strong disorder strength. blue circles  $W = 6$  ( $\xi \approx 2.85$ ), green squares  $W = 6\frac{2}{3}$  ( $\xi \approx 2.3$ ), red crosses  $W = 7\frac{1}{3}$  ( $\xi \approx 1.9$ ), turquoise dots  $W = 8$  ( $\xi \approx 1.6$ ), purple pluses  $W = 8\frac{2}{3}$  ( $\xi \approx 1.36$ ), green stars  $W = 9\frac{1}{3}$  ( $\xi \approx 1.17$ ), black rhombus  $W = 10$  ( $\xi \approx 1.02$ ).

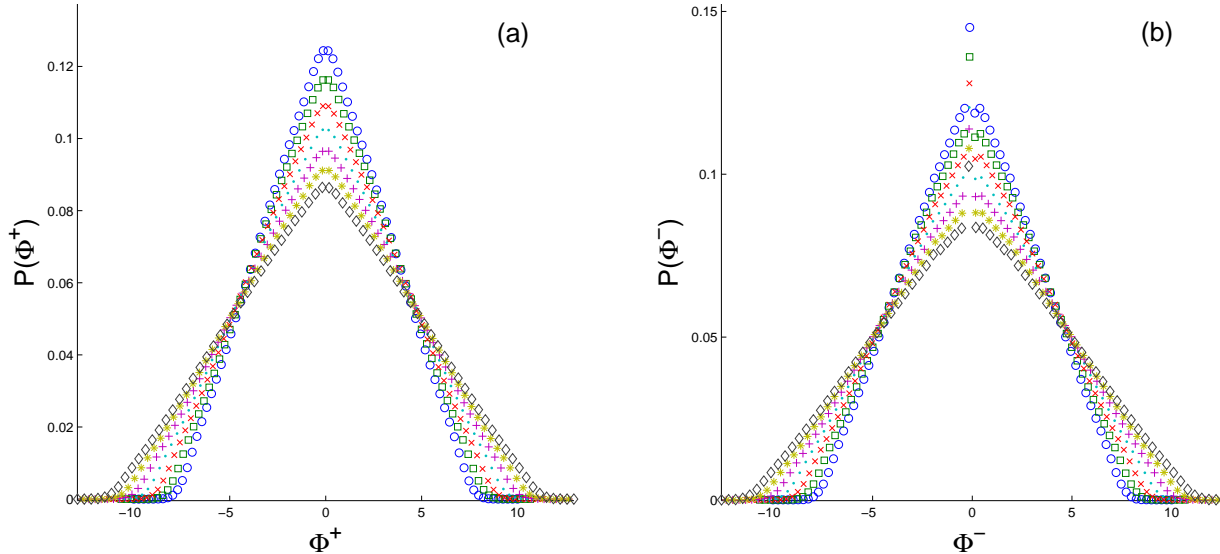


Figure 13: Distribution function in the regime of strong disorder. Symbols are as in Fig. 12. (a) The PDF of  $\Phi^+$ . (b) The PDF of  $\Phi^-$ .

## 5 Summary and Discussion

In this work the distribution function of some overlap sums  $V_{m_1}^{m_2, m_3, m_4}$  of (5) were calculated. In some cases of weak disorder it was demonstrated that scaling holds. In particular it was shown that for weak disorder (or large localization length  $\xi$ ) the distribution functions of  $V_0^{0,0,0}$ ,  $V_0^{0,1,1}$ ,  $V_0^{0,0,1}$  are functions of these variables and of  $\xi$  via one scaling variable,  $y_0 = \xi V_0^{0,0,0}$ ;  $y_1 = \xi V_0^{0,1,1}$  and  $y_2 = \xi^{3/2} V_0^{0,0,1}$  see (10), (15) and (18). The distribution function of  $y_0$  was calculated numerically (14). We could not find a scaling function for  $V_0^{0,1,2}$  and  $V_0^{1,2,3}$ . In addition to the fundamental interest, the scaling function can be extremely useful for the case when  $\xi$  is very large. It enables to obtain the distribution of  $V_{m_1}^{m_2, m_3, m_4}$  for regimes where numerical calculations require a basis of size that is beyond the available computer resources. Also the averages and variances of the  $V_{m_1}^{m_2, m_3, m_4}$  were computed for some  $\{m_i\}$ . In most cases of weak disorder we analyzed, these scale simply with  $\xi$  as one could guess from the distribution functions of the scaling variable. In some cases the averages are exponential in  $\xi$  (see Fig. 5).

The distribution functions of combinations of energies of the Anderson model were studied as well. A difference between  $\Phi^+ = E_n + E_m$  and  $\Phi^- = E_n - E_m$  was found near  $\Phi^+ = 0$ ,  $\Phi^- = 0$ . It is a signature of level repulsion. The distribution of  $\Phi_{m_1}^{m_2, m_3, m_4} = E_{m_1} + E_{m_2} - E_{m_3} - E_{m_4}$  was found to be gaussian and the dependence of the variance on the localization length was computed (21).

Some results for the various distributions were calculated in the regime of strong disorder. Results that are typically different from ones found for weak disorder were obtained.

The research can be continued in two directions. The distribution can be calculated numerically for additional cases and divided into classes with different characteristic properties. Also better analytical insights are called for.

This work was motivated by the effective noise theory for Nonlinear Schrödinger Equation (NLSE) in a random



potential [9, 7, 8] and the results of this work are of great importance for this theory. However the results may be of interest by themselves.

We would like to thank Y. Krivolapov for detailed discussions, extremely valuable technical detailed help and for extremely critical reading of the manuscript . This work was partly supported by the US-Israel Binational Science Foundation (BSF), by the Minerva Center of Nonlinear Physics of Complex Systems, and by the Shlomo Kaplansky academic chair.

## References

- [1] P. W. Anderson. Absence of diffusion in certain random lattices. *Phys. Rev.*, 109(5):1492, 1958.
- [2] P. A. Lee and T. V. Ramakrishnan. Disordered electronic systems. *Rev. Mod. Phys.*, 57(2):287–337, 1985.
- [3] S. Fishman, Y. Krivolapov, and A. Soffer. The nonlinear schrodinger equation with a random potential: results and puzzles. *Nonlinearity*, 25(4):R53, 2012.
- [4] S. Fishman, Y. Krivolapov, and A. Soffer. Perturbation theory for the nonlinear Schrödinger equation with a random potential. *Nonlinearity*, 22:2861–2887, 2009.
- [5] Y. Krivolapov, S. Fishman, and A. Soffer. A numerical and symbolical approximation of the nonlinear Anderson model. *New J. Phy.*, 12(6):063035, 2010.
- [6] G. Kopidakis, S. Komineas, S. Flach, and S. Aubry. Absence of wave packet diffusion in disordered nonlinear systems. *Phys. Rev. Lett.*, 100(8):084103, 2008.
- [7] S. Flach, D. Krimer, and Ch. Skokos. Universal spreading of wavepackets in disordered nonlinear systems. *Phys. Rev. Lett.*, 102:024101, 2009.
- [8] C. Skokos, D.O. Krimer, Komineas, and S. S. Flach. Delocalization of wave packets in disordered nonlinear chains. *Phys. Rev. E*, 79:056211, 2009.
- [9] E. Michaely and S. Fishman. Effective noise theory for the nonlinear schrödinger equation with disorder. *Phys. Rev. E*, 85:046218, 2012.
- [10] K. Ishii. Localization of eigenstates and transport phenomena in one-dimensional disordered system. *Suppl. Prog, Theor. Phys.*, 53(53):77–138, 1973.
- [11] I. M. Lifshits, L. A. Pastur, and S. A. Gredeskul. *Introduction to the theory of disordered systems*. Wiley, New York, 1988.
- [12] G. P. Agrawal. *Nonlinear fiber optics*, volume 4th. Academic Press, Burlington, MA ; London, 2007.
- [13] T. Schwartz, G. Bartal, S. Fishman, and M. Segev. Transport and Anderson localization in disordered two-dimensional photonic lattices. *Nature*, 446(7131):52–55, 2007.
- [14] Y. Lahini, A. Avidan, F. Pozzi, M. Sorel, R. Morandotti, D. Christodoulides, and Y. Silberberg. Anderson localization and nonlinearity in one-dimensional disordered photonic lattices. *Phys. Rev. Lett.*, 100(1):013906, Jan 2008.

- [15] F. Dalfovo, S. Giorgini, L. P. Pitaevskii, and S. Stringari. Theory of Bose-Einstein condensation in trapped gases. *Rev. Mod. Phys.*, 71(3):463–512, 1999.
- [16] L. P. Pitaevskii and S. Stringari. *Bose-Einstein condensation*. Clarendon Press, Oxford ; New York, 2003.
- [17] A. J. Leggett. Bose-Einstein condensation in the alkali gases: Some fundamental concepts. *Rev. Mod. Phys.*, 73(2):307–356, 2001.
- [18] L.P. Pitaevskii. Vortex lines in an imperfect Bose gas. *JETP*, 13(2):451–454, 1961.
- [19] E.P. Gross. Structure of a quantized vortex in boson systems. *Nuovo Cimento*, 20(3):454–477, 1961.
- [20] Y. V. Fyodorov and A. D. Mirlin. Level-to-level fluctuations of the inverse participation ratio in finite quasi 1d disordered systems. *PhysRevLett*, 71:412–415, 1993.
- [21] Roth Y. Cohen A. and Shapiro B. Universal distributions and scaling in disordered systems. *Phys. Rev. B*, 38:12125–12132, 1988.
- [22] B. Derrida and E. Gardner. Lyapounov exponent of the one dimensional anderson model : weak disorder expansions. *J. Phys. France*, 45(8):1283–1295, 1984.
- [23] H. Veksler, Y. Krivolapov, and S. Fishman. Double humped states in the nonlinear Schrödinger equation with a random potential. *Phys. Rev. E*, 81:017201, 2010.
- [24] A. Rivkind, Y. Krivolapov, S. Fishman, and A. Soffer. Eigenvalue repulsion estimates and some applications for the one-dimensional anderson model. *Journal of Physics A: Mathematical and Theoretical*, 44(30):305206, 2011.